EUROPEAN FUSION DEVELOPMENT AGREEMENT

EFDA–JET–PR(05)19

R.A. Pitts, J.P. Coad, D.P. Coster, G. Federici, W. Fundamenski, J. Horacek, K. Krieger, A. Kukushkin, J. Likonen, G.F. Matthews, M. Rubel, J.D. Strachan and JET EFDA contributors

Material Erosion and Migration in Tokamaks

Material Erosion and Migration in Tokamaks

R.A. Pitts[1], J.P. Coad[2], D.P. Coster[3], G. Federici[4], W. Fundamenski[2], J. Horacek[1], K. Krieger[3], A. Kukushkin[4], J. Likonen[5], G.F. Matthews[2], M. Rubel[6], J.D. Strachan[7] and JET EFDA contributors*

[1]Centre de Recherches en Physique des Plasmas, Association EURATOM-Conféderation Suisse, École Polytechnique Fédérale de Lausanne, CH-1015 Switzerland
[2]EURATOM/UKAEA Fusion Association, Culham Science Centre, Abingdon, OX14 3DB, UK
[3]EFDA-Close Support Unit, Garching, Boltzmannstrasse 2, D-85748 Garching bei München, Germany
[4]ITER Joint Central Team, Garching Joint Work Site, Garching D-85748, Germany
[5]Association EURATOM-TEKES, VTT Processes, P.O. Box 1608, 02044 VTT, Espoo, Finland
[6]Alfvén Laboratory, Royal Institute of Technology, Association EURATOM-VR, 100 44 Stockholm, Sweden
[7]PPPL, Princeton University, Princeton, NJ 08543, USA
** See annex of J. Pamela et al, "Overview of JET Results ", (Proc.20 [th] IAEA Fusion Energy Conference, Vilamoura, Portugal (2004).*

Preprint of Paper to be submitted for publication in
Nuclear Fusion

ABSTRACT

The issue of first wall and divertor target lifetime represents one of the greatest challenges facing the successful demonstration of integrated tokamak burning plasma operation, even in the case of the planned next step device, ITER, which will run at relatively low duty cycle in comparison to future fusion power plants. Material erosion by continuous or transient plasma ion and neutral impact, the susbsequent transport of the released impurities through and by the plasma and their deposition and/or eventual re-erosion constitute the process of migration. Its importance is now recognised by a concerted research effort throughout the international tokamak community comprising a wide variety of devices with differing plasma configuration, size and plasma facing component material. No single device, however, operates with the first wall material mix currently envisaged for ITER and all are far from the ITER energy throughput and divertor particle fluxes and fluences. This article aims to review the basic components of material erosion and migration in tokamaks, illustrating each by way of examples from current research and attempting to place them in the context of the next step device. Plans for testing an ITER-like first wall material mix on the JET tokamak will also be briefly outlined.

1. INTRODUCTION

In the low duty cycle ($\sim 10^{-2}$) devices constituting the bulk of modern research tokamaks, material erosion and its subsequent migration are of no practical operational consequence. This will not be so in the planned next step device, ITER (duty cycle of ~0.1) and certainly not in future fusion power plants operating continuously. In ITER, Plasma-Facing Components (PFCs) must satisfy the multiple demands of damage resistance due to high transient heat loads (such as ELMs and disruptions) lifetime as a result of plasma and neutral erosion and the requirement of low tritium retention [1].

The upscale from present machines to ITER in terms of stored energy, power exhaust, tritium throughput and plasma duration means that these demands extend far beyond those encountered in present machines. Extrapolating from JET, the largest currently operating tokamak, provides a striking example [2]: an entire JET campaign executed between 1999 and 2001 in the MarkIIGB divertor configuration provided an integral plasma duration in the divertor phase of ~14 hours (5478 discharges), with a total energy throughput of 220GJ and a divertor ion fluence of 1.8×10^{27}. This corresponds temporally to ~125 ITER discharges (400s diverted phase, $Q_{DT} = 10$ standard Type I ELM scenario [3]) but only ~ 4 ITER pulses scaled by energy input and only about one third of an ITER pulse in terms of expected divertor fluence.

Plasma fuel throughput will also increase dramatically in the next step, with ~50g of tritium expected to be injected during each full performance discharge, to be compared with only 0.01-0.2g per pulse in today's machines. If carbon PFCs are used in ITER (this is currently envisaged - Section 6), the high Tretention rates measured in present tokamaks (due to co-deposition as a result of C erosion and migration) extrapolate to 1-5g T retained per pulse, although these estimates are

still associated with substantial uncertainties. Assuming that carbon is used only in the divertor target area and, optimistically, that there will be no C migration to areas remote from the divertor, T-removal efficiencies in the range 90-98% will be required if premature replacement of the divertor before the erosion lifetime of 3000 full power DT pulses is to be avoided [4]. Such restrictions are imposed by nuclear licensing which, for safety reasons, limits the in-vessel T-inventory in ITER to ~350g [5]. Depending on the amount of T retained per pulse, as much as 100g T might need to be recovered overnight after each day of ITER full performance operation. This is 4 orders of magnitude higher than the 1-2g per month achieved on JET and TFTR, the only two tokamaks thus far to have performed DT experiments [6]. No active removal technique has yet been proven capable of releasing trapped tritium on any reasonable timescale and in the difficult ITER operating environment. Of all the processes driven by erosion and migration, fuel retention is possibly the greatest obstacle to be overcome if ITER is to be successful. It currently appears likely to exclude the use of carbon PFCs in the burning plasma phase.

The planned use of mixed materials (Be, C and W) in ITER finds no contemporary analog in modern devices, the majority of which operate with pure material PFCs (mostly C). Some experience has been gained on JET, where bulk Be tiles have in the past been used as divertor targets [7,8] and in which Be evaporation is routinely used for wall conditioning. The ASDEX-Upgrade tokamak has also been steadily acquiring experience with operation in a C+W environment as a precursor to future experiments with a full W wall and divertor [9,10]. However, ITER erosion and migration rates cannot be reproduced in these devices and there is growing concern that mixed material effects may lead to radical modifications to material properties. An example is the reduced melting temperature of BeW alloys which are expected to form when Be released from main chamber surfaces migrates to W divertor surfaces [11]. There are also potential difficulties associated with high T-retention in some cases (eg. in BeO [12]) compared with pure metals. Finally, enhanced physical sputtering erosion due to C/Be ion impact on C or W substrates is to be expected in comparison to yields due to hydrogenic ion bombardment alone (Section 2.1).

These and other issues drive the current effort towards an improved characterisation of erosion and migration processes [13]. Impurity migration can be broadly described in terms of a series of simple, but substantially inter-related components: erosion leading to impurity release, the transport of these impurities through and by the plasma and their redeposition. The latter may occur close to the point of erosion, or at remote locations. Re-erosion of deposited material is also possible, with subsequent further transport to regions no longer accessible to plasma or neutral species and where final deposition occurs. The extent of migration is dependent on material type (eg. high or low Z), plasma configuration (eg. limiter or divertor), plasma ion and neutral species, machine geometry and the importance of transient phenomena with respect to continuous erosion processes. In the following sections, each of these component processes will be individually described, using illustrative examples from the more recent literature.

2. EROSION

Continuous erosion of tokamak PFCs proceeds via physical and chemical sputtering (Section 2.1). Transient phenomena (Sections 2.3, 2.4) are also likely to be important contributors to erosion in next step devices and, if reliable methods compatible with performance goals cannot be found to mitigate them, may ultimately define PFC lifetimes. In tokamaks, the two most violent transient events that carry potential for severe first wall and divertor erosion are Edge Localised Modes (ELMs) and disruptions. Arcing, though ubiquitous during tokamak operation, has received little attention as an impurity production mechanism [1]. The same may be said for dust production via erosion processes, which is a concern for nuclear devices, where safety issues are important [1] and in which dust generation may scale up by several orders of magnitude in comparison to current devices. Some effort is now underway to model the dynamics of dust in tokamak plasmas [14, 15] and to develop diagnostic techniques for its observation. This modelling indicates that dust particulates can be swept into the plasma and travel long distances at high speed, providing a mechanism for long range migration.

2.1 FUNDAMENTAL EROSION PROCESSES

Physical sputtering is the most fundamental erosion mechanism in the sense that there is a finite probability for its occurrence whenever any incoming projectile (neutral or ionic) imparts sufficient energy to the surface atoms of any substrate to overcome their surface binding energy, of order a few eV for fusion relevant materials [16]. It is thus a threshold process, with a yield, Y_{phys}, that is strongly dependent on the mass ratio of target to projectile, since momentum transfer improves rapidly as the incoming particle mass approaches that of the target atoms. Figure 1(a) illustrates this threshold behaviour for deuterium bombardment of a range of fusion relevant materials and includes one particular ITER relevant case of C on W to demonstrate the dramatic increase in Y_{phys} for higher mass projectiles.

In a tokamak, ions reach PFCs with a directed average energy (in eV) of $E_i \sim 3Z_iT_e + 2T_i$, comprising respectively the energy gained via acceleration through the electrostatic sheath and the thermal energy. High charge state impurity ions leaving the confined plasma and arriving at surfaces before recombination to lower charge states may thus do so with significant energy. Indeed, without the cooling effect of a high recycling or detached divertor [18] (the mode in which the ITER divertor will operate [19]), higher mass impurities in the incoming ion flux could lead to uncontrolled sputter erosion. This is particularly true in the case of self-sputtering, whereby projectile and target masses are identical and for which Y_{phys} for high Z elements can considerably exceed unity.

In contrast to physical sputtering, chemical sputtering has an extremely low energy threshold and so will nearly always occur whenever chemically reactive species interact. Carbon is prodigiously employed in tokamaks as a result of its lack of a liquid phase (making it extremely forgiving under strong transient heat loads), its low Z (allowing larger core concentrations to be tolerated from the point of view of fuel dilution and radiation loss) and its extremely beneficial quality as an efficient radiator in the low temperature plasma edge regions (facilitating detachment and power dispersal).

In addition, the good thermomechanical properties (thermal condutivity and strength) of advanced

carbon materials (Carbon Fibre Composites (CFC)) make them attractive for fusion applications. Carbon, however, is also chemically active with the hydrogenic isotopes that constitute the fusion fuel. The resulting erosion places limits on PFC lifetimes even in ITER [1] and, more importantly, leads to strong T-retention due to co-deposition with eroded carbon.

There has been a great deal of progress over the last decade in the understanding of the fundamental reaction steps determining carbon chemical erosion, whose yield, Y_{chem}, depends on surface temperature, T_{surf}, incident projectile energy and flux and material properties [20]. Much of the original effort was, however, concentrated on ion beam experiments, which cannot access the low energies and high fluxes characteristic of the tokamak edge. Over the past few years, systematic in-situ measurements in tokamaks and plasma simulators have greatly expanded the database and a recent paper has attempted to regularise both ion beam and plasma data [21]. The principal result of this work is shown in Fig.1(b), which provides the flux dependence of Y_{chem} normalised to an incident energy of 30eV and where the data are taken, for the most part, near the maximum of the yield dependence on T_{surf}. There is a clear decrease in Y_{chem} at ITER divertor relevant fluxes of 10^{24} m^{-2} s^{-1} . When combined with the T_{surf} dependence in ERO Monte Carlo impurity transport code modelling, this Y_{chem} flux variation brings the predicted net chemical erosion rate near the divertor strike points (where power and particle fluxes and T_{surf} are highest) of an ITER pure C target down by an order of magnitude compared to usual estimates based on a fixed $Y_{chem} \sim 1.5\%$ [22]. Whilst significant, this reduction is still insufficient to prevent unacceptable tritium accumulation [23], even when accounting for the recent observation that Be impurities (which will migrate from an ITER all-Be first wall to divertor target surfaces) can impede C chemical erosion and hence reduce co-deposition [24].

2.2 STEADY STATE WALL EROSION

Even if physical sputtering at divertor targets can be largely suppressed under detached, or partially detached conditions, it will be the principal erosion mechanism at the tokamak main chamber walls, at least if carbon as wall material is avoided. An example for ITER is shown in Fig.2, where B2-Eirene code simulations have been used to compute the expected poloidal distribution of wall fluxes (due both to charge exchange (CX) D, T neutrals resulting from plasma recycling and gas puffing and D, T, He and impurity ions) and the subsequent material erosion due to sputtering, including chemical sputtering for a C wall [25]. The computed erosion rates in Fig.2(b) do not account for local redeposition, nor do they correctly model the ion outfluxes, which are known to be largely turbulent driven and cannot yet be predictively assessed for ITER. A recent experimental multi-machine study has, however, reported density dependent, overall particle fluxes to main chamber walls which are roughly independent of machine size [26].

Figure 2 clearly demonstrates the gain in lifetime offered by a high Z first wall - the maximum wall thinning is ~15 times lower in comparison to low Z materials. Total mass loss is however similar in all cases, amounting to about 1 ton per “full performance year” (namely, the gross erosion

that would result from 1 year of continuous, full power operation). Such erosion rates are acceptable for the low ITER duty cycle. The advantage of low erosion rates for high Z must be offset against the 3 orders of magnitude lower concentrations of high Z impurities that can be tolerated in the core plasma, particularly since wall eroded impurities are relatively poorly screened by the edge plasma in comparison to the divertor (Section 3). Experiments on ASDEX-Upgrade show, however, that the use of central heating (which fusion alphas will provide in ITER) can effectively prevent accumulation of W in the core plasma [9,10].

2.3 EROSION DUE TO TRANSIENTS: ELMS

In recognition of their potential for severe damage to divertor targets, Type I ELMs have been the subject of considerable study within the Fusion community in recent years. Efforts are being directed towards physics understanding [27-29], characterisation of ELM-induced PFC heat loads, erosion and damage [28, 30] and attempts to mitigate them or find small ELM regimes compatible with good confinement [29, 31-33]. Predictions for ITER have become increasingly sophisticated and less pessimistic, but are still marginal, even in the most optimistic case, with respect to divertor target ablation [28]. Part of the problem originates from the relatively weak scaling with machine size of both ELM duration and wetted area for power deposition.

Current extrapolations for ITER $Q_{DT} = 10$ reference conditions predict ELM plasma energy losses of between 3-8% of total stored energy (~350MJ) [28]. Accounting for the fact that only a part of the total ELM energy which arrives in the divertor does so in a time short enough to produce the sudden increase of T_{surf} at the targets, leads to expected energy fluxes at the ITER divertor targets in the range 0.6 - 3.4MJm^{-2} [28]. Figure 3 (a) demonstrates that only the lower end of this range would ensure that target thinning by ELM ablation does not reduce the minimum ITER divertor lifetime requirement (3000 full power pulses based on physical and chemical sputtering alone). A W target performs better than C, but the difference is marginal if 50% or more of the molten surface layer formed by the ELM heat pulse is lost as a result of electromagnetic forces [30].

The calculations in Fig.3(a) take no account of the statistical nature of ELM sizes [34], inner/outer divertor asymmetries in ELM power deposition [35] or the (potentially beneficial) impact of target vapour shielding and prompt redeposition of ablated material [30]. Nor do they account for ELM energy losses to main chamber surfaces which are now known to occur on a larger scale than initially suspected and have been directly observed [36].

The ELM begins as an MHD instability in the hot pedestal region localised on the outboard, or low field side of the torus [29] and, once released into the Scrape-Off Layer (SOL), appears to propagate radially, as a group of toroidally separated, rotating filaments of hot plasma convecting ions and electrons with energies characteristic of the pedestal plasma. The filaments lose energy rapidly parallel to the magnetic field but the speed of radial propagation can be such that ions, which cool slowly compared to electrons in the filaments, can reach wall and limiter surfaces with high energies. Figure 3(b) provides an example for Type I ELMs in the ASDEX-Upgrade, JET and

ITER tokamaks where a new transient model of ELM energy loss [37] has been used to compute the expected D^+ energies at first limiter surfaces (shown as distances from an assumed filament formation location halfway into the Hmode pedestal region). This model has been successfully tested against JET outboard limiter Langmuir probe measurements [38] and data from an ion energy analyser inserted into the JET far SOL [39]. It predicts an ion impact energy which scales strongly with machine size, such that some first wall ELM erosion would be expected on all devices for low Z walls (ie. low physical sputtering thresholds - Fig.1(a) and even for a high Z wall in larger tokamaks. For ASDEX-Upgrade, the model suggests that ELM wall ion energies would only be slightly above the W sputtering threshold and would thus be unlikely to erode W first wall components. This is consistent with measurements showing that fast neutral beam or ICRH generated ions with keV energies are by far the strongest contributors to impurity release from outboard W limiters during ELMing H-mode and not erosion due to background plasma ion impact [40]. The transient model predicts that only ~8% of the ITER ELM energy would deposit on outboard limiters [37] and this, coupled with the low ELM duty cycle, implies that ELMs will not be an issue for wall lifetime. Instead, as for the case with steady state erosion (Section 2.2), the lower screening for main chamber produced impurities may pose a core plasma contamination risk with high Z walls.

2.4 EROSION DUE TO TRANSIENTS: DISRUPTIONS

In comparison with ELMs, disruptions are less well characterised with regard to the spatial distribution and magnitude of power loading, due in part to the difficulty of the careful diagnosis required of a relatively rare and rapid event. A recent cross-machine study [41] provides more optimism for the next step than had been previously been the case [19], notably due to the finding that the plasma stored energy at the thermal quench is substantially lower than that during the full performance phase and that the thermal quench divertor power flux profiles are broader than initially thought. On the basis of the approximate scalings presented in [41], ITER divertor disruptive energy loads (expected average values of ~3.3 MJm^{-2} over a timescale of ~2.3ms) will be an order of magnitude lower than previously assumed, with a concomittant increase in the target lifetime, but will still be several factors above ablation limits of ITER candidate materials C and W. Disruption mitigation by massive gas puffing is therefore being actively pursued [42] as a method of spreading the energy load over the entire first wall and benignly terminating the discharge. It has also been suggested as a tool for detritiation by using the high stored energy of the ITER plasma to desorb tritium through transient heating of the near surface [43], although it is not clear that significant Be migration can be avoided due to large scale surface melting and subsequent droplet ejection due to $\mathbf{j \times B}$ forces.

3. TRANSPORT

Without transport in the plasma, often to locations far from the point of entry, impurities would have little or no influence on plasma behaviour. Core plasma impurity content, an important reactor concern, depends on the nature and location of impurity sources, their fuelling efficiency (or SOL and divertor

screening) and the impurity confinement once the core is reached [44]. Both impurity production and core transport are reasonably well characterised in comparison to SOL impurity transport [45]. The latter determines not only how well eroded material is screened from the core, but where it is eventually redeposited. In limiter machines (see also Section 5.1), the erosion of limiters tends to be the main impurity source and much of the eroded material is redeposited on these surfaces due to their proximity to the core plasma. In a divertor tokamak, impurities produced at divertor targets are generally far better screened (usually by factors of 3 or more [45, 46]) than those evolving from main wall surfaces - for example by CX fluxes, Fig.2 - a substantial fraction of which can nevertheless be transported directly down the SOL into the divertor regions (see below).

Impurities produced locally within the divertor region are ionised and may then promptly return to the target plates or be transported through the divertor plasma. The extent to which either occurs depends principally on the competing influence of ion temperature gradient forces (∇T_i), driving impurities out of the divertor and frictional drag with fuel ion flows, directed towards the strong particle sink imposed by the targets [18]. Fluid flows driven by classical drifts may also convect particles from one divertor leg to another [47]. They are primarily due to E×B terms and have been measured [48, 49], but their influence on impurity entrainment remains unclear, nor is it clear to what extent divertor (and SOL) flows simply close upon themselves without any net particle transport. The degree of prompt redeposition, in the divertor and elsewhere, is dependent not only on local plasma parameters, but also on the impurity particle itself; high Z impurities are usually so easily ionised and have comparatively large larmor radii that they can be promptly re-deposited [50]. Unfortunately, the situation is more complex in the case of C, for which the combination of low Z, plasma chemistry and complex erosion pathways can lead to longer range migration and strong sensitivity to local plasma conditions (Section 4).

In the SOL, ∇T_i forces and plasma flows also exist, with the latter having recently become the subject of rather intense experimental activity [49, 51, 52]. Matthews (see Fig.6 in [17]) has provided a useful compilation of recent experimental measurements of parallel SOL particle flows from a number of divertor tokamaks, obtained exclusively using Langmuir Mach probe techniques under L-mode conditions. To these must be added very recent data from ASDEX-Upgrade [53,54] and TCV [55]. In the divertor regions these flows are directed with sonic speeds to the target plates. In the SOL, for the toroidal field direction usually employed in tokamak research (ie. with ion B×∇B drift directed towards a lower X-point and thus favourable for H-mode access), qualitatively similar parallel flows are observed to circulate in the direction from outer to inner divertor on all machines. They do so with parallel flow speeds, $v_{||}$, that can exceed $M_{||} = 1$ (where $M_{||} = v_{||}/c_s$ with c_s the ion sound speed), as measured, for example, in the inboard midplane far SOL in C-Mod [51]. It is just in these regions radially distant from the separatrix that efficient collisional coupling is possible between the background flow and any impurities produced at main chamber walls and limiters [46], leading to the suspicion that SOL flows can be responsible for material migration from main chamber to divertor areas.
Although 2D edge fluid codes (SOLPS5, EDGE2D/Nimbus, UEDGE) including classical drifts can

qualitatively reproduce the observed poloidal (and to some extent radial) flow patterns [49, 52, 56, 57], the predicted magnitude in the SOL is too low to produce any significant migration. The observation on C-Mod that the strong inboard midplane flows remain unchanged upon field reversal [51], directly implies a further missing component in the physics model. This has been suggested in [51] as being due at least partly to ballooning transport favouring the outboard regions, though implementation of such transport with varying strength in the fluid codes is still unable to reproduce the measured flow strength [58, 59]. It is interesting to note that a similar ballooning contribution was proposed much earlier as one mechanism by which strong parallel flows in the limiter tokamak DITE might be explained [60].

Ultimately, the migration patterns that are observed in the divertor are due to a combination of SOL and local divertor transport, deposition and re-erosion. In addition, such patterns are usually observed by post-mortem analysis of target surfaces and are thus often integrated over long experimental campaigns comprising a large number of discharge types and strike point locations. To separate these effects, at least partially, a great deal of effort has recently been devoted to the use of tracer injection experiments, pioneered on TEXTOR tokamak [61] for local (limiter) transport studies, but now employed on all major divertor tokamaks [62-66]. In most cases, ^{13}C labelled methane ($^{13}CH_4$) is introduced into a series of identical discharges via gas puffing at a given poloidal location and, if possible, toroidally uniformly. The experiments are performed at the end of experimental campaigns so that tiles may be extracted and their surfaces analysed using sensitive ion beam techniques [67] which can detect extremely low concentrations of the tracer. Figure 4 compiles some of the results obtained using this technique from the DIII-D, ASDEX-Upgrade and JET tokamaks, illustrating the diversity of injection locations and plasma conditions that have been investigated thus far.

For the case of injection from the top of the poloidal cross-section into ohmic or L-mode conditions, both JET and DIII-D report similar findings [62,64]. Although typically only ~50% or less of total injected ^{13}C can be accounted for by post-mortem surface analysis, the majority of that found is deposited inboard of the inner strike point (Fig.4 (a,b)). This is similar to what is seen in long term C migration patterns (Section 4) and is at least partially due to the outer to inner divertor parallel SOL flows mentioned above. Indeed, through a combination of extensive experimental data and modelling tools, the DIII-D results have been shown to be entirely consistent with impurity flows of $M_{||} \sim 0.4$ throughout the SOL towards the high field side [69,70], though these flows were imposed in the simulations. A similar modelling exercise for JET, produced reasonable qualitative agreement with the measured inner target ^{13}C deposition profile, but could not reproduce the observed 99:1 inner/outer target ^{13}C ratio [71].

In ASDEX-Upgrade, ^{13}C injected from the outer midplane into an ELMing H-mode deposited rather symmetrically (1.5:1 in favour of the outer divertor) at both strike points (Fig.4(c)) and, in the strike point areas, is distributed in a similar way to that found in long term C deposition data [65, 72]. Away from the strike point, and particularly at the inner divertor, ^{13}C accumulates on the top of the inner baffle, possibly a result of the ubiquitous strong outer to inner SOL flow. However, this feature

is not present in long term distributions, which also exhibit a wing of increased deposition outside the inner strike point area, shifting the deposition balance 2.5:1 in favour of the inner divertor [72]. These are indications for the importance of an intrinsic C source outside the divertor and point to important differences between a punctual exposure over a few discharges in which transport to the divertor is important, rather than deposition-erosion and redeposition operating over a longer term campaign.

Interpretation of the very recent results [67] in Fig. 4a for toroidally continuous outer divertor injection into 39 identical JET ELMing H-modes (analysis of data for Tile 6 is incomplete at the time of writing) has yet to be attempted. There are differences in comparison to the long term C-migration patterns (Fig.5(a)), in particular the lower inner target deposition and the increased outer target deposition. A similar experiment on ASDEX-Upgrade (injection location shown in Fig.4(c)) injected much smaller quantities from a toroidally localised gas puff (0.0025g compared with 9.3g in JET) into 12 Type I ELMing H-modes and found, within experimental errors, that all the injected ^{13}C was deposited locally downstream of the injection point with a spatial distribution consistent with the local magnetic field line direction and an added E×B drift [66]. In JET, analysis thus far finds (toroidally integrating the results of analysis at a single toroidal location) ~10% of the injected ^{13}C at the inner target and ~13% at the outer. There is also evidence (using a collector probe in the main chamber) both for escape of ^{13}C out of the divertor and preferential flow from outer to inner target [67]. The effect of ELMs on this transport has yet to be assessed.

The ^{13}C divertor concentration profiles compiled in Fig.4 are an interesting demonstration of how the migration can appear both simple and extremely complex. The challenge to theory is now to understand how transport leads to such distributions.

4. DEPOSITION AND RE-EROSION

In all present devices, the tokamak inner divertor is a region of net deposition, with the outer a zone of net erosion or neutral erosion/redeposition [1, 73]. This is due in part to the prevalence for a colder, more dense inner divertor and a hotter outer divertor, both driven by the effect of toroidal geometry (more power conducted to the outboard side), increased outboard transport rates and drifts which deposit power preferentially into the outer divertor [57]. It also appears to be a consequence of the main chamber in tokamaks being generally a zone of net erosion [17, 74], such that impurities eroded there can be swept into the divertors, presumably aided by the strong flows discussed in Section 3.

An example of the long term erosion/deposition is shown for JET in Fig.5(a), obtained by post mortem mechanical (micrometer) measurements following the MarkIIGB divertor operation phase [75]. There is little net erosion or redeposition at the outer target (with the exception of strong deposition on the horizontal base tile - see below), but strong deposition at the inner, pointing to a net main chamber C source. In DIII-D (upper part of Fig.5(b)), long term net erosion has been observed at the outer target, with net deposition at the inner [73], behaviour seen also in JT-60U [76] and ASDEX-Upgrade [72]. In contrast, during high density, deuterium fuelled detached divertor operation

in DIII-D (lower part of Fig.5(b)), a sample manipulator inserted into the divertor detected net deposition everywhere [77], providing further evidence for a source outside the divertor region under these conditions. The situation can be reversed by instead detaching the divertor plasma radiatively using neon injection; the high physical sputter yield of neon ions is then a major contributor to the subsequent large net erosion measured at the outer divertor [78].

When high Z materials are used in the divertor, similar features are generally observed in the local erosion redeposition patterns, but the situation is usually complicated by the presence of mixed materials. Hence, the ASDEX-Upgrade Divertor I configuration, with W targets but C in the main chamber, observed net erosion at the outer target due mainly to W physical sputtering by C fluxes [79]. At the inner target, enhanced C deposition rates effectively coated the W surface, preventing further erosion and providing further evidence for a main chamber erosion source. High density operation reduced erosion even in the hotter outer target region due to prompt local redeposition as a consequence of extremely short ionisation lengths for the eroded W.

In the all-Mo C-Mod tokamak, very low outer target erosion rates have been reported [80], amounting to only 0.14nm/s or 0.45cm/year (contrast this with the DIII-D outer target C erosion rate in Fig.5(b)). Even these are attributed mostly to enhanced low Z impurity physical sputtering, mainly due to boron introduced as a result of wall conditioning. Elsewhere in the divertor, erosion rates were considerably lower, a consequence both of surface coating by boron, and the high density operation characteristic of C-Mod, leading to very low divertor plasma temperatures.

Many of these results demonstrate how sensitivity to local plasma conditions is an important factor in determining the rate of divertor erosion or deposition, particularly in the case of carbon. Whilst hotter, less dense attached plasmas promote increased sputter yields, in colder regions commonly found in the inner divertor, physical sputtering is all but suppressed and only chemical erosion (in the case of C) operates. That the local erosion/deposition balance can switch according to plasma conditions is nicely demonstrated (Fig.5(c)) by a recent reversed toroidal field campaign in JET [57]. Infra Red thermography (IR) measurements of the divertor targets revealed that the anomalous surface temperature increases always seen at the inner target during transient events, occurred also at the outer target after several 10's of reversed field discharges [81]. These IR anomalies are attributed to the presence of surface carbon layers with thermal properties that differ from the bulk material and thus appeared to grow also at the outer target, disappearing again over time when the normal field direction was restored. Field reversal was also accompanied by a radical switch in the SOL parallel flow patterns [57] and degree of symmetrisation of outer and inner divertor plasma parameters [82]. The degree to which the shift in deposition was due to a modified C source rate into the divertor legs (as a consequence of the SOL flow redistribution) or a change in the divertor plasma parameters (itself likely due to mostly to drift flows) remains to be clarified and represents a challenge to modelling. Specifying a plasma temperature dependent C erosion mechanism (as seen, for example, in EDDY code studies [83]) in SOLPS5 fluid- Monte Carlo code simulations (including drifts) of the JET divertor has recently been successful in explaining the strong outer to inner deposition asymmetry shown in Fig.5(a) [58].

The fact that deposited carbon layers (or indeed any layer containing mixed material) cannot be simply treated as an extension of the underlying substrate is a complicating factor in determining the final erosion/deposition distribution, particularly when modelling long term measurements. In addition, it is no surprise to find that geometry can play an important role in migration. Both aspects are illustrated by the example in Fig.5(d) showing real time deposition measurements obtained on a shot resolved basis with a novel Quartz MicroBalance (QMB) diagnostic [84] mounted at the entrance of the JET inner divertor pumping duct. In this sequence of H-mode ELMing discharges in the so-called diagnostic optimised magnetic configuration (DOC), the inner strike point was moved progressively further down the vertical targets, placed finally on the horizontal plate and subsequently alternated between the two [85]. Deposition on the QMB increases by a factor 9 as the strike point approaches the inner vertical corner and then by a further factor 3 upon first contact with the base plate, on which direct plasma interaction is rather rare in this JET divertor configuration. The interpretation of this latter observation calls for erosion of a soft C layer which is formed by gradual migration of material eroded during repeated operation with the more common vertical strike points to a region with little or no plasma contact. These amorphous hydrocarbon layers on the horizontal base tiles are readily identified in the deposition profile of Fig.5(a). Thermal decomposition of these layers is also implied by strong increases in molecular light emission (C2 and CD) which are observed when strike points are placed in the inner corner region [86].

Much of the carbon eroded from this remote area by plasma impact has a direct line of sight to the QMB, demonstrating the importance of geometry in determining deposition rates. Modelling of the ensemble of this QMB data with the 3D Monte Carlo ERO impurity transport code has been rather successful, but only if performed under the assumption of enhanced C re-erosion yields in the surface layers compared to the bulk material [85]. The validity of this assumption has been clearly demonstrated by dedicated ^{13}C injection experiments through a test limiter in TEXTOR [87], whilst the increased erosion rates for a:C-H layers compared with bulk carbon have been known for some time from laboratory experiments [88].

The combination of high inner target deposition rates, stepwise migration due to enhanced reerosion, geometry effects and the added requirement for high sticking of neutral hydrocarbon molecules at the point of first contact in remote areas [88] would seem to provide a substantial part of the explanation for the high C deposition, leading to the formation of macroscopic carbon flakes that have been found on the water cooled louvers of the JET inner divertor pumping duct [89]. It was in these very flakes that a significant fraction of the in-vessel retained tritium was found following the JET DTE1 campaign [89].

5. GLOBAL MIGRATION ACCOUNTING

Accounting for the movement of material over the complex in-vessel structures of modern tokamaks, often over long experimental campaigns comprising thousands of discharges, is no trivial task. It is nevertheless being increasingly attempted [17, 74] and Fig.6 summarises pictorially the results of

three such studies.

5.1 LIMITER TOKAMAKS

To date, the most rigorous balance has been achieved for C in TEXTOR (prior to the installation of the Dynamic Ergodic Divertor) using extensive post mortem surface analysis of a large number of in-vessel components [74, 90 and references therein] - Fig. 6a. Not surprisingly, the carbon toroidal belt limiter is the main C source, amounting to ~22g/hour through chemical and physical sputtering. Limiter surface temperatures are at least 350^{o}C, with plasma ion temperatures in the range 50-200eV, generally much higher than those in colder divertor plasmas. The main chamber wall is erosion dominated by CX sputtering [91]. Redeposition occurs again mostly at the main limiter (~10g/hr.) with smaller rates to obstacles in the SOL intercepting field lines perpendicularly, to the inner bumper limiter and to the neutraliser plates under the toroidal limiter. About 1-2g/hr. are pumped out in the form of stable hydrocarbons and a much smaller quantity (0.02g/hr.) is found along the pump ducts (at room temperature) in the form of soft, hydrogen rich hydrocarbon layers reminiscent of the deposits observed at the JET inner pump duct (Section 4) and in the ASDEX-Upgrade sub-divertor region [91]. Total deposition+loss thus amounts to 19-20g/hr. and is in remarkably good balance with the total erosion given the experimental uncertainties. A full year of continuous TEXTOR operation under the conditions appropriate to this migration study would thus yield a total carbon movement of ~175kg.

In Tore Supra, a similar balance has been attempted, but is not as complete as the TEXTOR study [92]. Erosion from the toroidal pumped limiter is estimated from spectroscopic measurements to be in the range ~11-29g/hr., similar to TEXTOR values, but the balance cannot yet be closed with deposition since a large fraction of deposits are thought to lie in regions below the limiter which are inaccesible without removing major water cooled components [93]. Nevertheless, estimates of the total D inventory trapped in the C (~20g) presently unaccounted for do not provide more than a third of that necessary required to explain the large in-vessel fuel retention observed on Tore Supra [92].

5.2 DIVERTOR TOKAMAKS

Migration of C and Be during the MkIIGB divertor phase of JET has been quantified by checking for consistency between total estimated wall sources and the total divertor deposition [2,17]. The latter is obtained from campaign averaged, post mortem surface analysis [94], whilst the former is extracted using EDGE2D/Nimbus code simulations to calibrate spectroscopic measurements (of BeII and CIII light) along specific lines of sight against the modelled wall source for a wide range of JET discharges [46]. It has also been predicted using measurements of core Z_{eff} in combination with experimental screening factors determined by CD_4 gas puffing [46]. Both approaches predict main wall erosion rates of ~1ton per year of continuous high performance JET operation [17], with a divertor C source ~10 times higher, assumed to be due to multiple C recyling in the divertor

before loss to remote areas.

The result of this accounting is shown in Fig.6(b), where main chamber C and Be quantities are well balanced by estimated divertor deposition found essentially all at the inner (see also Fig.5(a)). Unlike C, Be does not erode chemically and is detected only on the vertical target tiles, highly enriched (Be:C > 10:1) throughout the deposit. The much lower quantity of Be compared with C also reflects that fact that it is only present through evaporation onto main chamber surfaces using discrete sources. This divertor deposition extrapolates to ~215kg (C) and 12kg (Be) for a year of continuous operation.

At the time of writing, the ASDEX-Upgrade C migration picture is still unclear [72]. Earlier studies with an all-C heat shield [74], concluded that erosion at the inner column was likely the main C source for the observed inner divertor deposition. This was not supported, however, by subsequent operation in 2001 with a W-coated inner heat shield, during which spectroscopic observations indicated that the C outer poloidal limiters were likely the primary main chamber C-erosion source [95]. Eroded impurities were being transported to the W inner column and undergoing multiple recycling steps there before being lost to the inner divertor. More recent operation during the 2002-2003 campaign, with a further increase in of the in-vessel W-coated surface area (though still with C divertor targets - see Fig.6(c)) and during which the divertor target erosion and deposition have been measured, has revealed substantial net erosion sources in the outer divertor which closely balance the net deposition observed at the inner target [72]. Main chamber erosion sources during this campaign are estimated to be more than an order of magnitude too small to account for the inner divertor deposition. These observations would therefore appear to contradict the picture of a main chamber impurity source concluded for JET and seen earlier in ASDEX-Upgrade itself. There is, however, no evidence from the outer divertor $^{13}CH_4$ puff experiment in ASDEX-Upgrade (Section 3) for net C transport from outer to inner divertor. This inevitably casts some doubt on the observation of balanced divertor erosion/redeposition and there is indeed a suspicion that the special marker layers deposited on the divertor tiles and used to measure the erosion might have delaminated at the outer target due to the high heat fluxes experienced there [72]. New experiments are underway to clarify the ASDEX-Upgrade C balance, but it is worth noting that the total inner divertor C deposition measured during the 2002-2003 campaign extrapolates to the same value for continuous operation (~215kg/year) as that found in JET!

The same campaign has been used to assess W migration, with the result shown in simplied form in Fig.6(c) (extracted from [96]). Of the total gross erosion (due only in this case to physical sputtering) measured on the W-coated heat shield, a large fraction (~2/3) occurs during the limiter phases during start up and ramp down, and is promptly redeposited. Only in the divertor phases can W eroded from the inner column migrate to the targets and here the balance is far from closed, with only ~12% of the estimated main wall W erosion being found at the targets, corresponding to ~1.5kg/year for continuous operation and thus >100 times lower than seen for C. In further contrast to the case for low Z impurities, W divertor deposition is found to distribute almost equally between

inner and outer targets at a rate (~4% of the wall erosion rate) close to that with which W is estimated to penetrate the core plasma. Strong deposition on the inner divertor baffle indicates direct transport along field lines connecting divertor and heat shield, whilst the missing 88% of divertor phase W erosion would appear to be promptly redeposited on the inner column. Only with detailed modelling, however, can such a qualitative analysis be confirmed.

6. TESTING EROSION AND MIGRATION WITH AN ITER-LIKE FIRST WALL IN JET

As shown in Fig. 7, the current ITER materials choice is an all Be-clad first wall, W over much of the divertor region and CFC only at the target plates themselves where the highest power fluxes are expected [97]. This materials combination is driven by the need for operational flexibility, but has never been tested in an operating tokamak. Even with the area of CFC reduced to a minimum, T-retention by co-deposition remains the major concern associated with the use of carbon and ITER maintains an option to switch from CFC to W targets prior to DT operation depending on findings during the initial years of operation in H/D plasmas. This is possible due to a flexible divertor design employing removable and reuseable cassettes. The same is not true for the first wall armour, which could only be replaced at very substantial cost and time penalties.

In support of ITER with regard to this difficult question of material choice, an ambitious programme of JET upgrades has recently been approved, preparations for which are now underway and with which first operation is projected in 2009 [98]. A major component of this upgrade will be the installation of an ITER-like first wall, with two options presently under consideration (Fig. 7). Option 1, the favoured starting alternative if sufficiently robust W coatings can be developed, tests a full W coated CFC divertor, matching the ITER fallback (second phase) option. Option 2 matches the ITER primary choice, but suffers from the potential for contamination of the pure Be wall should C be observed to migrate in large quantities from the divertor. This would make it more difficult later to continue experiments with Option 1, but at the same time would provide valuable input for ITER.

Dedicated experiments with the new wall on JET will aim to address a large number of the issues raised in the introductory remarks and discussion throughout this paper. For the Be wall, the primary interest will be characterisation of the nature and magnitude of main chamber erosion, both during and in-between ELMs and during disruptions. In the latter case, the accompanying additional heating power upgrade [98] should allow access to ITER-relevant disruption energy densities and hence also testing of mitigation schemes. Proper migration accounting is equally important to allow more reliable extrapolation of expected Be accumulation rates in the ITER divertor. Once in the divertor, the effects of Be deposition on C or W release can be studied under realistic conditions of surface temperature and plasma impact, including transient loads. If sufficient power is available to produce ELM energy release in the region of 2MJ, then melt layer loss studies on a W divertor become accessible. There is already evidence on JET that 1MJ ELMs are sufficient to drive C ablation. Transients of this magnitude will provide a realistic environment in which to gauge the damage evolution of mixed surface layers

and possibly to study the effect of BeW alloying on reducing the W melting point. Both CFC and W plasma facing surfaces in the ITER divertor modules are castellated for stress relief [99], providing a large number of gaps into which it is feared that material, particularly C, may migrate, exacerbating the Tretention problem [100]. Castellated test modules are envisaged during operation with the new JET wall to investigate this possibility.

CONCLUDING REMARKS

Though of no operational significance in current tokamaks, material erosion and migration will be important players in ITER and beyond, where core plasma performance and wall lifetime issues cannot be decoupled. Unfortunately, the combination of exposure to a wide range of plasma conditions, often in the same device, a variety of machine and magnetic geometries, complex and frequently poorly understood transport, mixed materials, violent transient events, insufficient diagnostics and the considerable upscale in performance, timescales and fluence from the majority of today's tokamaks to ITER make extrapolation a rather perilous exercise. The importance of migration is nevertheless now recognised and activity within the research community is increasing as ITER approaches. Considerable effort is still required, however, to refine predictive capability through improved experiment and models and to pursue full wall materials tests in relevant environments.

ACKNOWLEDGMENTS

For his detailed reading of the manuscript and helpful suggestions, S. Brezinsek is gratefully acknowledged. This work was supported in part by the Swiss National Science Foundation, EURATOM and the UK Engineering and Physical Sciences Research Council and performed under the European Fusion Development Agreement.

REFERENCES

[1. Federici G et al 2001 *Nucl. Fusion* **41** 1967
[2]. Matthews G F et al 2003 Material Migration in JET *Proc 30th EPS Conference on Contr. Fusion and Plasma Phys. (St. Petersburg), Europhys. Conf. Abstracts* **27A**, P-3.198
[3]. Technical basis for the ITER final design, ITER-EDA Documentation Series, No. 24 (IAEA Vienna 2002)
[4]. Skinner C H, Federici G 2005 accepted for publication in Physica Scripta
[5]. Technical basis for the ITER final design, ITER-EDA Documentation Series, No. 24, *Radiological Source Terms*, Chap. 5.3 (IAEA Vienna 2002)
[6]. Skinner C H, Coad J P, Federici G 2004 *Physica Scripta* **T111** 92
[7]. Thomas P R, JET Team 1991 *J. Nucl. Mater.* **176&177** 3
[8]. Loarte A et al 2005 *J. Nucl. Mater.* **337-339** 816
[9]. Neu R et al 2005 *Nucl. Fusion* **45** 209
[10]. Kallenbach A et al 2005 *these proceedings* paper I3.004

[11]. Doerner R P, Baldwin M J, Causey R J 2005 *J. Nucl. Mater.* **342** 63
[12]. Causey R A, Walsh D S, J. Nucl. Mater. 254 (1998) 84
[13]. Philipps V, Roth J, Loarte A 2003 *Plasma Phys. Control. Fusion* **45** A17
[14]. Krasheninnikov S I et al 2004 *Phys. Plasmas* **11** 3141
[15]. Krasheninnikov S I et al 2005 *these proceedings* paper P4.019
[16]. Bohdansky J 1984 *Nucl. Fusion Special Issue* 61
[17]. Matthews G F 2005 *J. Nucl. Mater.* **337-339** 1
[18]. Stangeby P C 2000 The Plasma Boundary of Magnetic Fusion Devices, IoPP
[19]. ITER Physics Basis, 1999 *Nucl. Fusion* **39** 2137
[20]. Roth J 1999 *J. Nucl. Mater.* **266-269** 51
[21]. Roth J et al 2004 *Nucl. Fusion* **44** L21
[22]. Roth J et al 2005 *J. Nucl. Mater.* **337-339** 970
[23]. Kirschner A et al 2005 *these proceedings* paper P1.013
[24]. Schmid K, Baldwin M, Doerner R P 2005 *J. Nucl. Mater.* **337-339** 862
[25]. Behrisch R et al 2003 *J. Nucl. Mater.* **313-316** 388
[26]. LaBombard B et al 2000 *Proc 18th IAEA Fusion Energy Conf. (Sorrento),* **IAEA-CN-77/EX5/6**
[27]. Becoulet M et al 2003 *Plasma Phys. Control. Fusion* **45** A193
[28]. Loarte A et al 2004 *Phys. Plasmas* **11** 2668
[29]. Huysmans G T Y 2005 *these proceedings,* paper I4.002
[30]. Federici G, Loarte A, Strohmayer G et al 2003 *Plasma Phys. Control. Fusion* **45** 1523
[31]. Lang P T 2005 *these proceedings,* paper 04.003
[32]. Saibene G et al 2005 *Nucl. Fusion* **45** 297
[33]. Evans T E et al 2004 *Phys. Rev. Lett.* **92** 235003
[34]. Loarte A et al 2002 *Plasma Phys. Control. Fusion* **44** 1815
[35]. Eich T et al 2005 *J. Nucl. Mater.* **337-339** 669
[36]. Herrmann A et al 2004 *Plasma Phys. Control. Fusion* **46** 971
[37]. Fundamenski W, Pitts R A submitted to *Plasma Phys. Control. Fusion*
[38]. Fundamneski W et al 2005 *these proceedings,* paper P2.013
[39]. Pitts R A et al submitted to *Nucl. Fusion*
[40]. Dux R et al 2005 *these proceedings,* paper P1.040
[41]. Loarte A et al 2004 *Proc 20th IAEA Fusion Energy Conf. (Vilamoura), paper IT/P3-34*
[42]. Whyte D et al 2003 *J. Nucl. Mater.* **313-316** 1239
[43]. Whyte D, Davis J W 2005 *J. Nucl. Mater.* **337-339** 560
[44]. Strachan J D et al 2004 Nucl. Fusion **44** 772
[45]. Pitcher C S, Stangeby P C 1997 *Plasma Phys. Control. Fusion* **39** 779
[46]. Strachan J D et al 2003 *Nucl. Fusion* **43** 922
[47]. Chankin A V 1997 *J. Nucl. Mater.* **241-243** 199
[48]. Bodeo J A et al 2000 *Phys. Plasmas* **7** 1075

[49]. Asakura N et al 2004 *Nucl. Fusion* **44** 503
[50]. Naujoks D 1997 *Nucl. Fusion* **37** 1193
[51]. LaBombard B 2004 *Nucl. Fusion* **44** 1047
[52]. Erents S K et al 2004 *Plasma Phys. Control. Fusion* **46** 1757
[53]. Tsalas M et al 2005 *these proceedings,* paper P2.001
[54]. Müller H W et al 2005 *these proceedings,* paper P1.009
[55]. Pitts R A, Horacek J *in preparation*
[56]. Bonnin X et al 2005 *these proceedings,* paper P2.110
[57]. Pitts R A et al 2005 *J. Nucl. Mater.* **337-339** 146
[58]. Coster D P et al 2004 *Proc 20th IAEA Fusion Energy Conf. (Vilamoura), paper TH/P5-18*
[59]. Kirnev G et al 2005 *J. Nucl. Mater.* **337-339** 271
[60]. Pitts R A et al 1990 *J. Nucl. Mater.* **176&177** 893
[61]. Wienhold P et al 2001 *J. Nucl. Mater.* **290-293** 362
[62]. Likonen J et al 2003 *Fus. Eng. Design* **66-68** 219
[63]. Rubel M et al 2005 *these proceedings,* paper P2.004
[64]. Allen S et al 2005 *J. Nucl. Mater.* **337-339** 30
[65]. Vainonen-Ahlgren E et al 2005 *J. Nucl. Mater.* **337-339** 55
[66]. Pugno R et al 2005 *J. Nucl. Mater.* **337-339** 985
[67]. Rubel M et al 2005 *Vacuum* **78** 255
[68]. Wampler W R et al 2005 *J. Nucl. Mater.* **337-339** 134
[69]. McClean A G et al 2005 *J. Nucl. Mater.* **337-339** 124
[70]. Elder J D et al 2005 *J. Nucl. Mater.* **337-339** 79
[71]. Strachan J D et al 2004 *Proc 30th EPS Conference on Contr. Fusion and Plasma Phys. (London), Europhys. Conf. Abstracts* **28G**, P-1.136
[72]. Mayer M et al 2005 *J. Nucl. Mater.* **337-339** 119
[73]. Whyte D et al 1999 *Nucl. Fusion* **39** 1025
[74]. Mayer M et al 2004 *Physica Scripta* **T111** 55
[75]. Coad J P et al 2003 *J. Nucl. Mater.* **313-316** 419
[76]. Gotoh Y et al 2003 *J. Nucl. Mater.* **313-316** 370
[77]. Whyte D et al 2001 *Nucl. Fusion* **41** 1243
[78]. Wampler W R et al 2003 *J. Nucl. Mater.* **313-316** 333
[79]. Krieger K et al 1999 *J. Nucl. Mater.* **266-269** 207
[80]. Wampler W R et al 1999 *J. Nucl. Mater.* **266-269** 217
[81]. Andrew P et al 2005 *J. Nucl. Mater.* **337-339** 99
[82]. Huber A et al 2005 *J. Nucl. Mater.* **337-339** 241
[83]. Ohya K et al 2004 *Physica Scripta* **T111** 138
[84]. Esser H G et al 2003 *Fus. Eng. Design* **66-68** 855
[85]. Kirschner A et al 2005 *J. Nucl. Mater.* **337-339** 17

[86]. Brezinsek S et al 2005 *J. Nucl. Mater.* **337-339** 1058
[87]. Kirschner A et al 2004 *J. Nucl. Mater.* **328** 62
[88]. von Keudell A et al 1999 *Nucl. Fusion* **39** 1451
[89]. Coad J P et al 2001 *J. Nucl. Mater.* **290-293** 224
[90]. von Seggern J et al 2003 *J. Nucl. Mater.* **313-316** 439
[91]. Rohde V et al 2004 *Physica Scripta* **T111** 49
[92]. Dufour E et al 2005 *these proceedings,* paper P5.002
[93]. Brosset C, Khodja H, Tore Supra team 2005 *J. Nucl. Mater.* **337-339** 664
[94]. Likonen J et al 2005 *J. Nucl. Mater.* **337-339** 60
[95]. Pütterich T et al 2003 *Plasma Phys. Control. Fusion* **45** 1873
[96]. Krieger K et al 2005 *J. Nucl. Mater.* **337-339** 10
[97]. Federici G et al 2003 *J. Nucl. Mater.* **313-316** 11
[98]. Lioure A et al, Preparing ITER with JET, *to be presented at the 21st Symposium on Fusion* Engineering, 26-29th September 2005, Knoxville, Tennessee, USA
[99]. Daenner W et al 2002 *Fus. Eng. Design* **61-62** 61
[100].Rubel M et al 2004 *Physica Scripta* **T111** 112

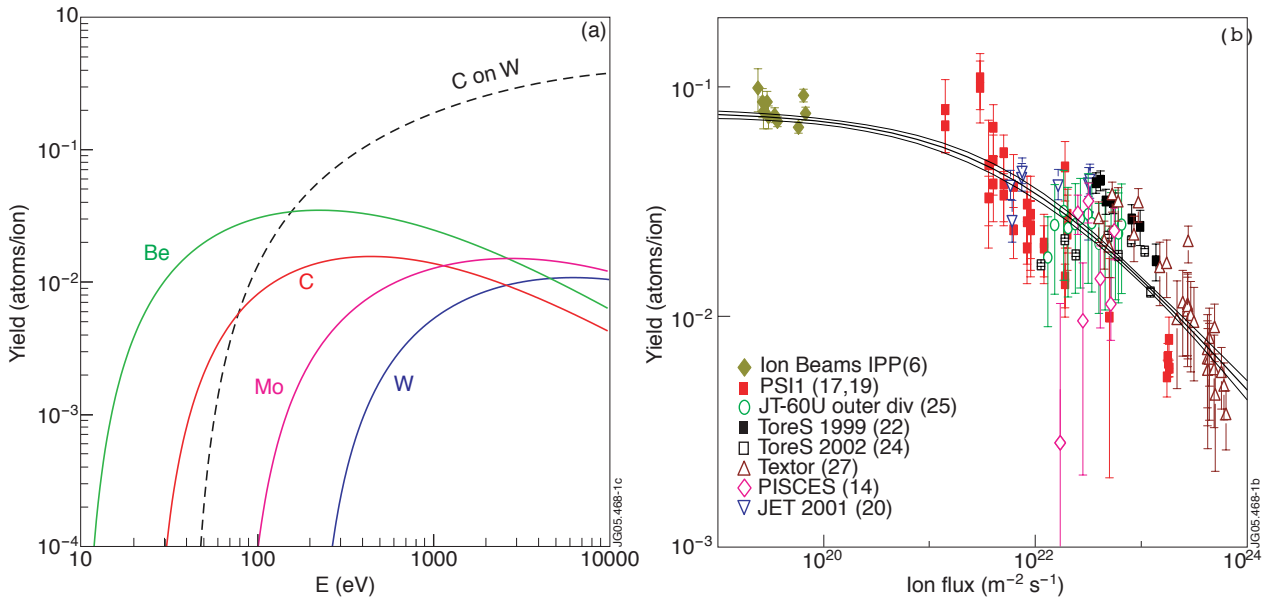

Figure 1: Fundamental tokamak erosion processes: a) Physical sputtering, shown for normal incidence deuterium impact on various fusion relevant substrates (adapted from [17]), with an example of C on W illustrating the strong yield dependence on projectile mass, b) Chemical sputtering - from a recent attempt [21] to regularise experimental data from a variety of sources for the yield dependence on particle flux density.

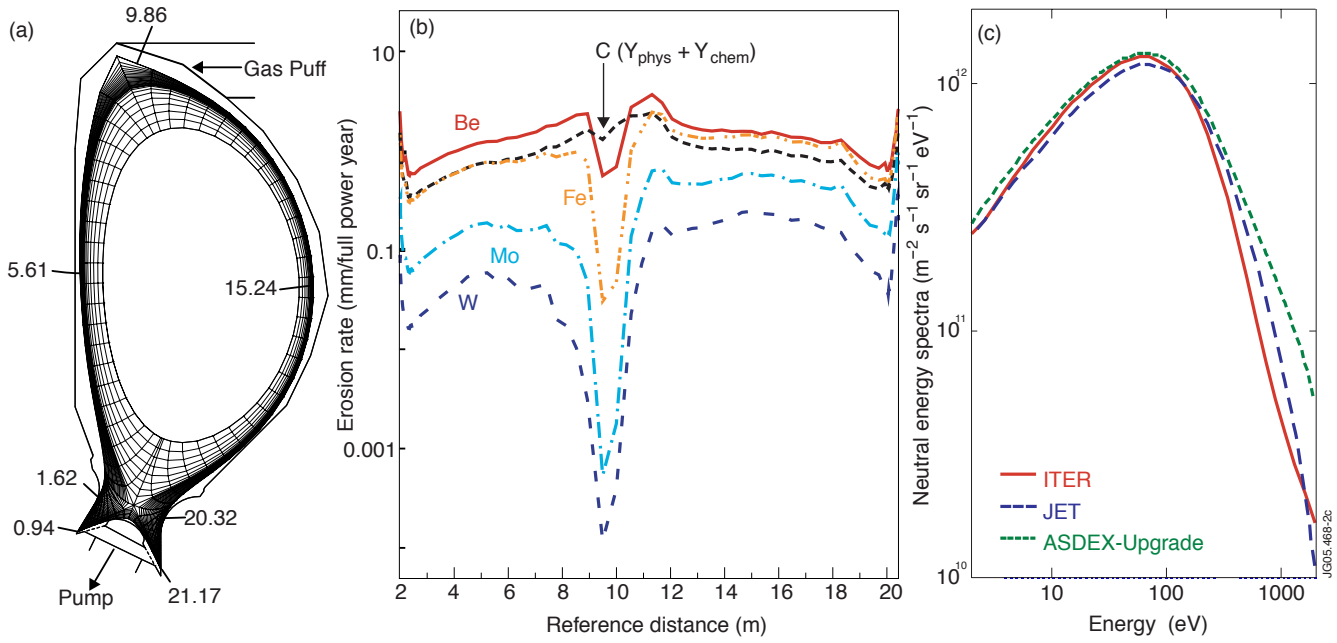

Figure 2: Simulated ITER wall erosion for continuous operation: a) B2-Eirene ITER simulation grid with reference poloidal distances for identification of locations on the abcissa of b) which compiles calculated erosion rates for various first wall choices due to physical sputtering by D, T, He and impurity ions and neutrals. c) CX neutral energy spectra at the outside midplane from B2-Eirene Hmode simulations on ASDEX-Upgrade, JET and ITER demonstrating the similarity in all three cases - a consequence of the CX spectrum being dominated by wall recycled neutrals which typically penetrate only to edge regions where $T_e \sim 100$eV before ionisation and susbsequent chargeexchange. (a,b) adapted from [25]. CX spectra from ASDEX-Upgrade in c) supplied by Y. Chen.

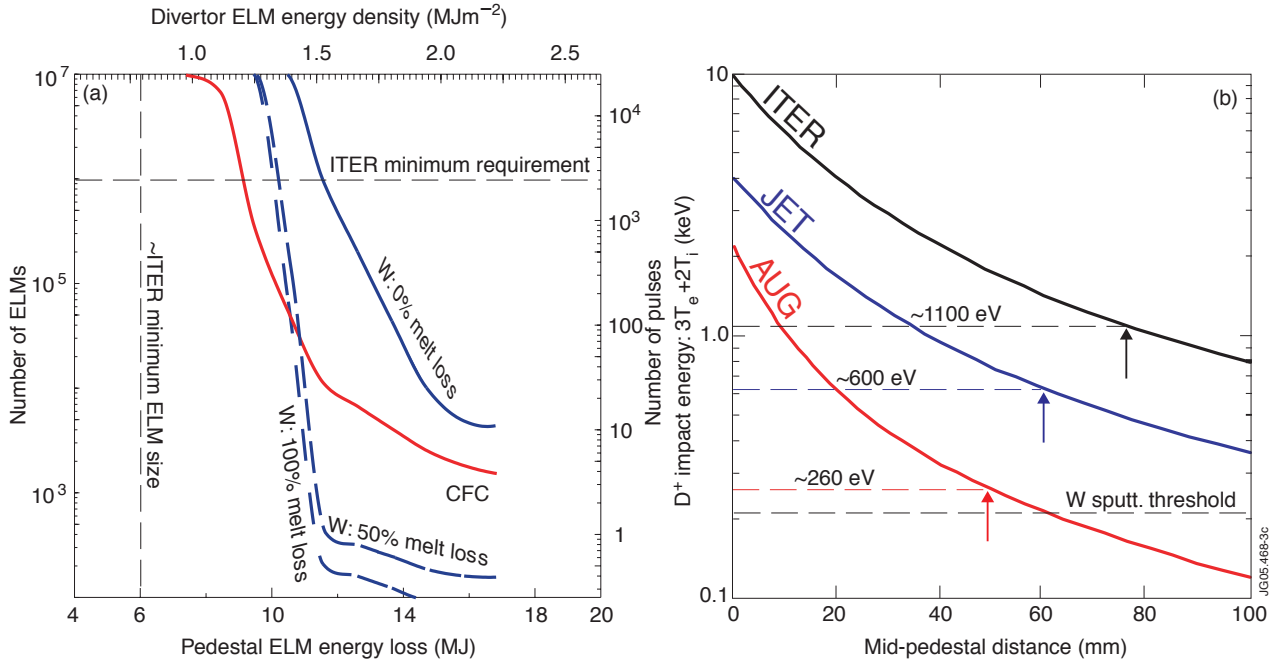

Figure 3: ELM erosion: a) predicted CFC (20 mm starting thickness) or W (10mm thickness) divertor target lifetime due to ablation expressed in terms of number of ELMs or number of full power ITER pulses ($f_{ELM} = 1Hz$) as a function of pedestal energy loss per ELM or divertor energy density for an inter-ELM power density of 5 MWm^{-2} and including the case of 0, 50% or 100% melt layer loss for W (adapted from [30]). b) estimates, based on a new transient parallel loss model [37] of expected ELM ion energies at the main chamber limiter radius (marked by vertical arrows) for Type I ELMs in high power ASDEX-Upgrade and JET H-modes and in the ITER reference H-mode. Note, for example, that $Y_{phys} = 0.5\%, 1.0\%$ for impact of 1.1keV D,T on W respectively.

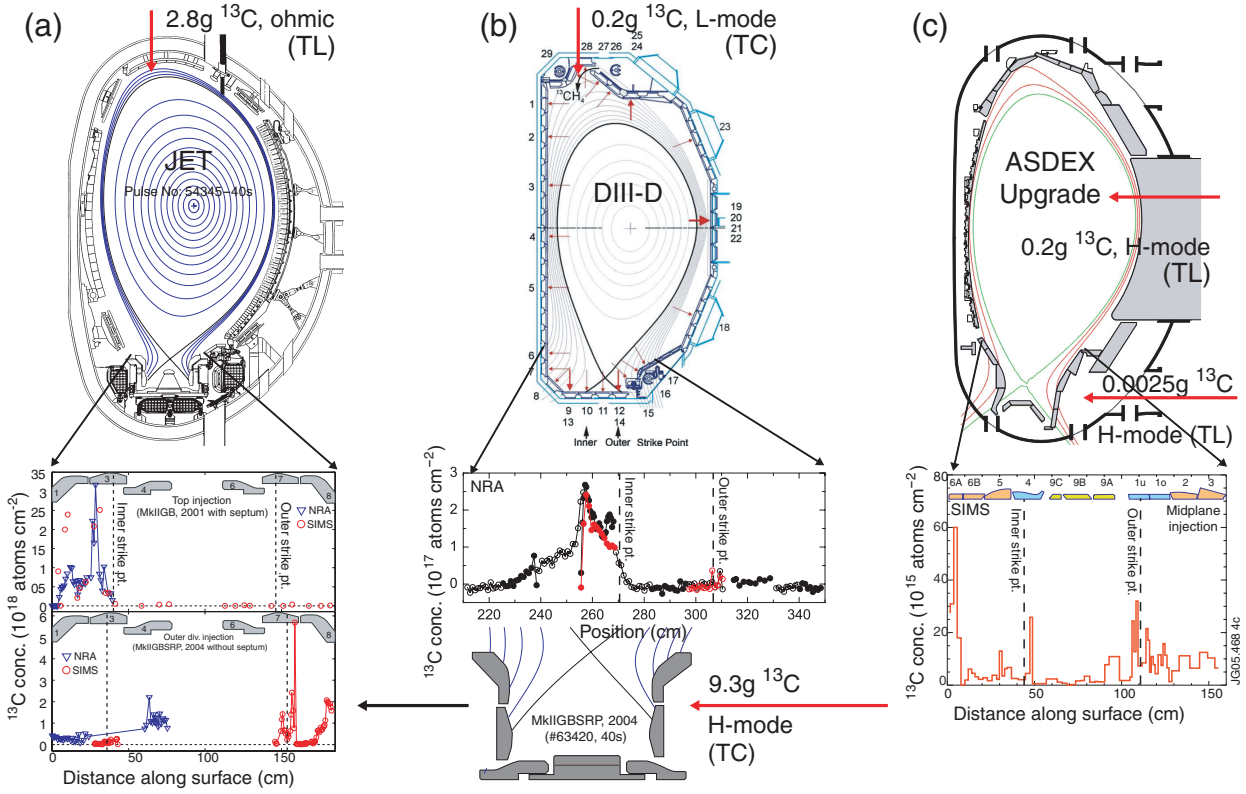

Figure 4: Compilation of ^{13}C tracer injection results from a) JET [62, 63], b) DIII-D [68] and c) ASDEX-Upgrade [65]. Arrows on the poloidal cross-sections indicate injection locations, injection quantities and plasma conditions. TL and TC denote, respectively, "toroidally localised" and "toroidally continuous" injection. Profiles of divertor "^{13}C surface concentration are shown in the lower part of each figure (SIMS: Secondary Ion Mass Spectrometry, NRA: Nuclear Reaction Analysis). All experiments with conventional B_ϕ direction. Note that the ASDEX-Upgrade midplane and outer divertor injections were made into the same discharges but that the outer divertor ^{13}C profiles are not shown (see text).

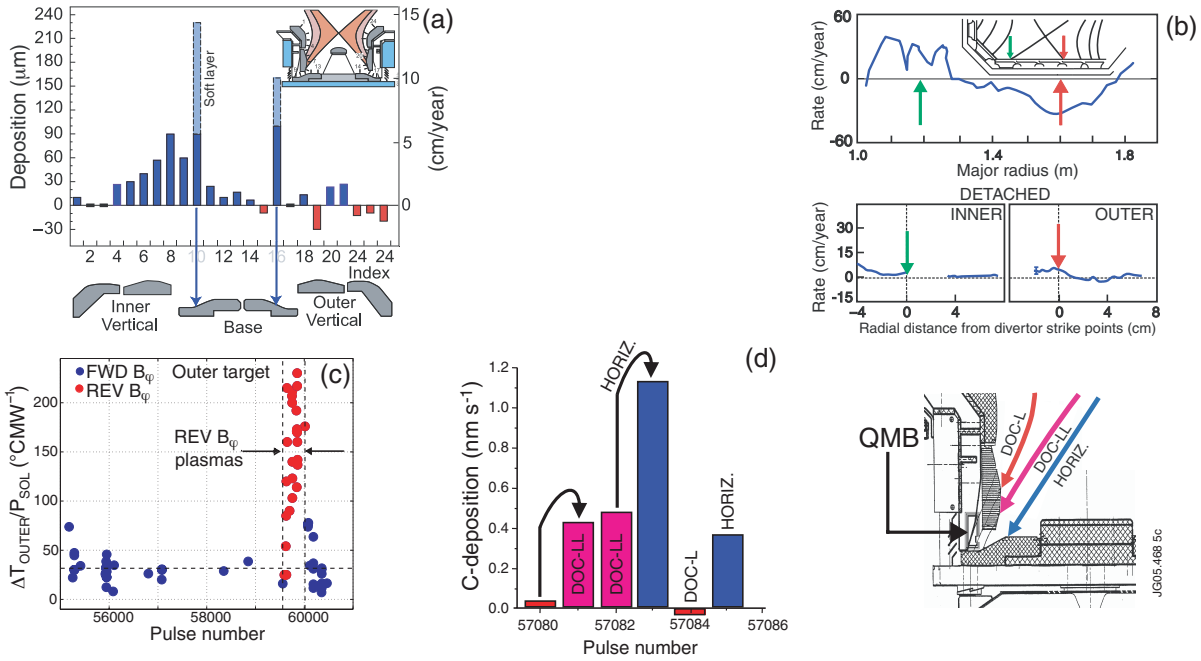

Figure 5: Compilation of JET and DIII-D data illustrating deposition and re-erosion: a) long term C deposition in the JET MarkIIGB divertor phase (adapted from [17,75]), b) divertor detachment can switch the erosion-deposition balance in DIII-D (adapted from [73,77], c) toroidal field reversal in JET switches divertor plasma asymmetry and promotes net outer target deposition with a subsequent larger rise of the apparent IR measured surface temperature in response to power load steps (see text for more details - from [57]), d) divertor strike point position can strongly influence C migration in JET (adapted in part from [86]).

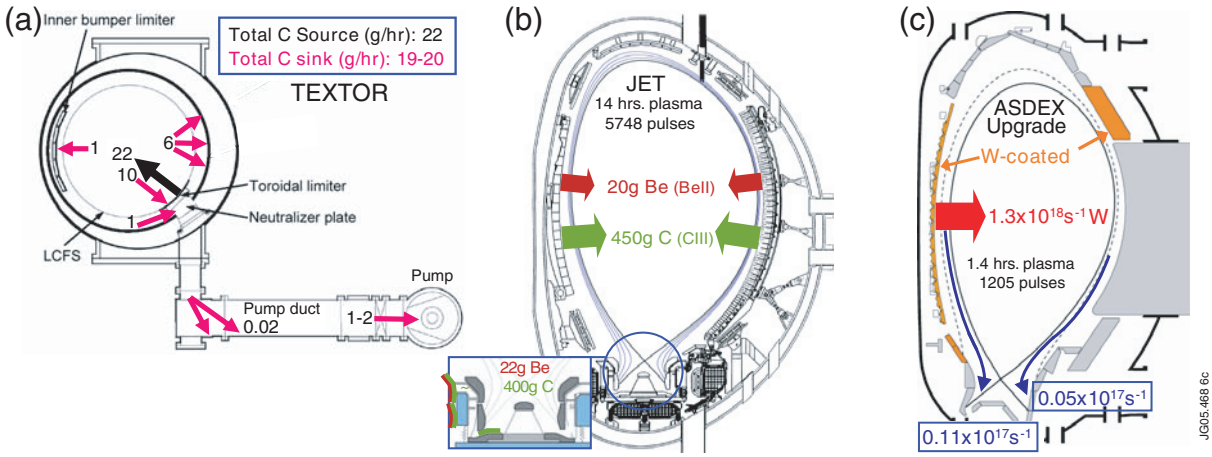

Figure 6: Three examples of long term global migration accounting: a) C-balance for the limiter tokamak, TEXTOR with erosion and redeposition rates given in g/hour [90], b) C and Be accounting for the JET MkIIGB divertor 1999-2001 campaign (from [17,94], c) W accounting for the ASDEXUpgrade 2002-2003 campaign (adapted from [96]). Total plasma durations quoted for JET and ASDEX-Upgrade are for the diverted phases only.

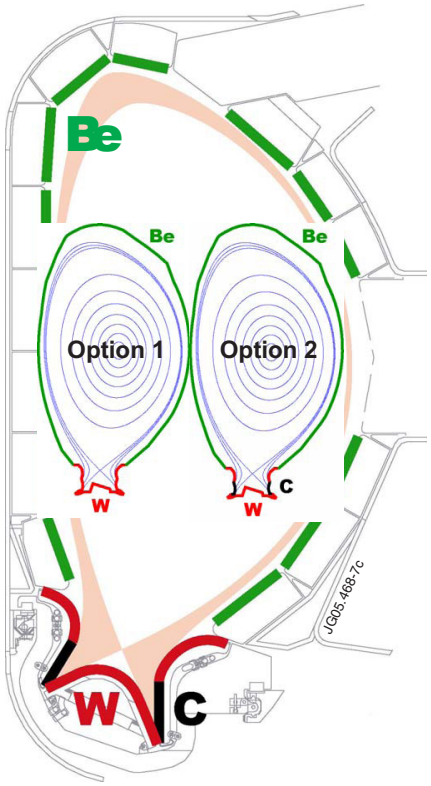

Figure 7: Current first wall material mix forseen in ITER with the two options currently under study for a new ITER-like wall at JET. Note that the JET poloidal cross-sections are to scale (ITER major radius = 6.2m, JET = 2.96m). With the accompanying additional heating power upgrade (providing 40-45MW of total power), JET is expected to reach a maximum of ~20MJ stored energy, to be compared with 350MJ in a full performance ITER reference scenario.